ACS APPLIED MATERIALS & INTERFACES

Research Article

www.acsami.org

Schottky Barrier Thin Film Transistors Using Solution-Processed *n*-ZnO

Ahmad H. Adl, Alex Ma, Manisha Gupta, Mourad Benlamri, Ying Y. Tsui, Douglas W. Barlage, and Karthik Shankar*

Department of Electrical & Computer Engineering, University of Alberta, Edmonton, AB T6G 2 V4 Canada

Supporting Information

ABSTRACT: Solution-processed ZnO thin films are attractive as active materials in thin film transistors (TFTs) for low-cost electronic device applications. However, the lack of true enhancement mode operation, low mobility, and unreliability in transistor characteristics due to the high density of traps and other defects present challenges in using such TFTs in circuits. We demonstrate in this report that the electrical characteristics of such TFTs can be improved by source injection barriers. Asymmetrical Schottky source metal−oxide−semiconductor field-effect transistors (MOSFETs) have been fabricated by utilizing heavily doped solution-processed ZnO as the active layer. n^+-ZnO was obtained by using triethylamine as the stabilizer in the solution process instead of the more commonly used monoethanolamine. Au was chosen for source metallization to create a Schottky contact to the ZnO and an Al ohmic contact was chosen as the drain. Voltage applied to the gate induced field emission through the Schottky barrier and allowed modulation of the drain current by varying the width of the barrier. By operating the asymmetrical MOSFET when the Schottky contact is reverse biased, effective control over the transistor characteristics was obtained.

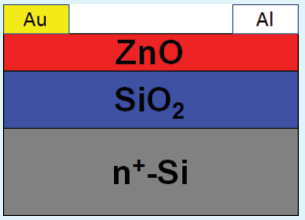

KEYWORDS: *thin film transistor, solution processing, sol−gel zinc oxide, Schottky junction, asymmetrical MOSFET, source injection barrier*

1. INTRODUCTION

Solution processing is a relatively inexpensive, high-throughput, manufacturing method on large area substrates and is particularly desirable for the fabrication of low-cost electronic and optoelectronic devices. ZnO is a wide band gap semiconductor made from earth-abundant materials. It has a combination of promising optoelectronic properties including a large exciton binding energy, high radiation resistance, good electronic mobility, high breakdown field, high saturation velocity, and facile solution-based synthesis.[1−3] These properties render ZnO thin films attractive as active layers in solution processed FETs for use in low-cost electronic displays, radio frequency identification tags, power inverters, light-emitting devices and transparent electronics.[4−6] In addition, *n*-ZnO, in conjunction with *p*-type semiconducting thin films of organic small molecules and polymers, can be used to construct circuits that implement complementary logic.[7,8]

Currently, the two solution-processing methods commonly used to form ZnO thin films are pyrolysis of a coated film of a solution-based ZnO precursor (usually zinc acetate)[9] and the spin-coating of a colloidal dispersion of ZnO nanoparticles, subsequently subjected to sintering.[6,7] In both these methods, it is difficult to control the electrical parameters of the films such as the doping density and defect concentration from run to run, and *p*-type ZnO is not yet reproducibly obtainable.[10] Therefore, better methods to control the electrical characteristics of the FETs incorporating ZnO films are much needed.[11−15] Furthermore, a moderately doped ZnO active layer is ideal in order to modulate the threshold voltage for low-power applications. However, solution-processed ZnO films are unintentionally heavily *n*-doped with typical carrier concentrations in the 1×10^{17} to 1×10^{18} cm^{-3} range. In addition, most ZnO TFTs are undesirable depletion mode devices requiring a negative gate voltage to turn off the device.[16−19] Thus, control of the threshold voltage in ZnO TFTs is highly desirable.[11] In this communication, we report on an asymmetrical thin film transistor using solution processed ZnO with a Schottky barrier source metal contact and an ohmic drain contact. We demonstrate that the electrical characteristics of the resulting *n*-MOSFETs can be more effectively controlled in this configuration.

2. EXPERIMENTAL PROCEDURE

The precursor solution consisted of zinc acetate dihydrate (Fisher Scientific) mixed with triethylamine (99%, Sigma-Aldrich) in a 1:1 ratio. 2-Methoxyethanol (99%, Acros Organics) was added to make 100 mL of the solution. The solution was stirred and heated at 120 °C for 4 h until it became transparent. Two solutions of 0.1 and 0.25 M zinc acetate were made using this recipe and spin coated on to 200 nm thick thermally grown oxide-coated n^+-type silicon wafers. The n^+-Si/SiO_2 substrates were dried at 130 °C. Subsequently, they were annealed at 500 °C for 90 min. This process was repeated three times. The 0.1 M, 0.25 M, and 0.25 M solutions were used for each cycle, respectively. The thickness of the film measured using ellipsometry was 46 nm and confirmed by stylus profilometry to be ∼50 nm. Film

Received: December 1, 2011
Accepted: March 3, 2012
Published: March 4, 2012

morphology was imaged using a Hitachi S-4800 cold cathode high resolution field emission scanning electron microscope (FESEM). Au and Al were used as the Schottky and ohmic contacts respectively. Metallization was performed using DC sputtering on photolithographically patterned substrates. A three step photolithography process was used to define the electrodes including a mesa step to electrically isolate individual TFTs. X-ray diffraction (XRD) patterns were collected from the ZnO films at glancing incidence using a Rigaku Ultima IV diffractometer. The electrical characteristics of the ZnO devices were measured on a Signatone Probe Station using a Keithley 4200-SCS semiconductor parameter analyzer.

3. RESULTS AND DISCUSSION

3.1. Film Growth. It is known from several prior studies that the temperature and duration of pre- and postannealing processes determine the orientation of ZnO films prepared using zinc acetate as the precursor, monoethanolamine as the stabilizer and 2-methoxyethanol as the solvent.[20−26] The effect of the precursor is well-studied with reports showing that zinc nitrate results in a rough dendritic film morphology with smaller grain sizes compared to zinc acetate, which results in smoother, larger-grained films.[27] Likewise, it is also known that higher precursor concentrations[28] and higher boiling point solvents favor larger grain sizes. However, the effect of stabilizer on the properties of films has not been explored yet. We used triethylamine (TeA) as the stabilizer in the solution growth process because of its ability to coordinate to Zn^{2+} ions and prevent premature methathesis reactions. The TeA adduct of dimethylzinc is widely used as a precursor for the growth of ZnS, ZnSe and ZnO.[29] TeA also assists in the hydrolysis of zinc acetate to form ZnO. The XRD patterns collected from the ZnO thin films are shown in Figure 1 and indicate three major

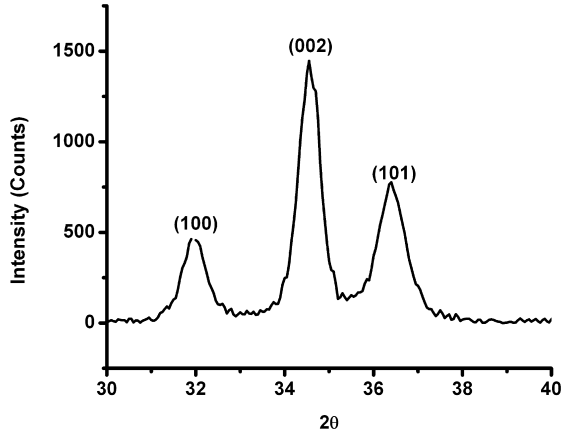

Figure 1. X-ray diffractogram of ZnO film. Three peaks observed for sol−gel ZnO: (100), (002), (101). The (002) peak is not dominant and the film lacks preferential texture. Using Scherrers formula, a grain size of 16 nm was estimated.

peaks: (100), (002), and (101), which are commonly observed for solution-processed ZnO. In order to achieve better crystallinity, the preheating method proposed by Ong et al[30] was used for annealing the ZnO films. This method is reported to generate ZnO films with a preferred (002) orientation, which results in better charge transport.[30] The replacement of monoethanolamine (MEA) by TeA as the stabilizer in our process significantly influenced the doping and crystallinity of the film. The ZnO films no longer possess a preferred orientation as can be seen in Figure 1. This shows that the result obtained by the preheating annealing method is sensitive to the recipe used. We also found that the order of making the precursor solution has a key impact on the doping of the film. When the zinc acetate is wet by TeA first with subsequent addition of the methoxyethanol, films with high *n*-type doping result whereas if TeA is added to the mixture of zinc acetate and methoxyethanol the doping is low resulting in near intrinsic films. We attribute to this to the different local environments for the Zn^{2+} cations in the two cases mentioned above. Ordinarily, Zn^{2+} ions are surrounded by a Coulombic hydration sheath even in methoxyethanol. However, when zinc acetate dehydrate is wet by triethylamine first, the hydration shell is disrupted by the deprotonation of the water molecules by the triethylamine.[31]

An FESEM image of the morphology of the obtained ZnO film is shown in Figure 2. The lateral grain size was observed to

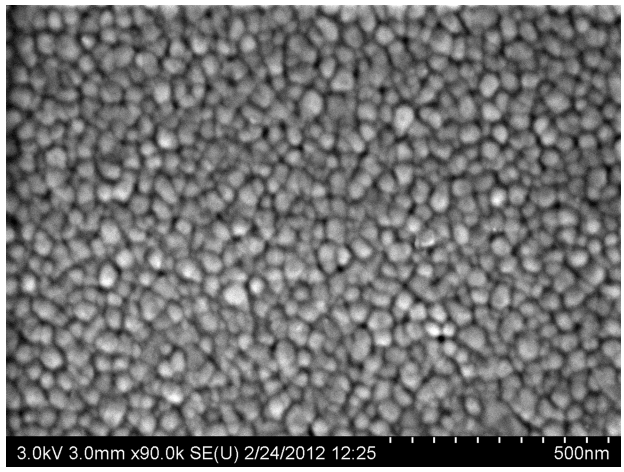

Figure 2. FESEM image of the morphology of the ZnO film. The film is continuous with no pores or cracks. The grain size is 15−40 nm.

be 15−40 nm from the FESEM image while the value deduced from XRD measurements using the Scherrer equation was found to be 16 nm. Since the ZnO film was formed in a sequence of 3 cycles as indicated in the experimental details in Section 2, we surmise that smaller grains closer to the interface are obtained in the first cycle using lower concentration ZnO precursor, which are responsible for the peak broadening in the XRD pattern. These grains act as nucleation sites for larger grains that form in the subsequent cycles using higher concentration ZnO precursor. These larger grains constitute the top surface of the film imaged by FESEM. As can be seen from the image, the surface of the film is very smooth with no cracks and pores. Compared to results obtained in the literature with MEA as the stabilizer, the ZnO films grown by us using TeA as the stabilizer have smaller grain sizes and are less orientated in the [002] direction. Because the *c*-axis is the most facile direction of growth for ZnO, we infer from the FESEM and XRD results that the complexation of zinc cations with TeA results in a lower nucleation barrier and a higher crystallization barrier when compared to complexation with MEA. This is likely due to the differences in bonding and boiling points between the two stabilizers (b.p. = 170 °C for MEA and b.p. =89 °C for TeA).[32]

3.2. Device Configuration and Theory of Operation. FETs employ the field effect of the gate to modulate the conductance of the channel between two ohmic contacts. The FET is in saturation when the semiconductor channel is

pinched off at the drain. Metal-semiconductor field-effect transistors (MESFETs) offer higher channel mobilities than metal−insulator−semiconductor field-effect transistors (MISFETs) due to lower scattering at the semiconductor-gate dielectric interface but present the problem of a higher leakage current. Schottky barrier gate electrodes have been used in ZnO MESFETs to retain the advantage of high mobility while decreasing the leakage current.[33] In contrast, Schottky barrier thin film transistors (SB-TFTs) use a Schottky contact as the source or drain electrode to limit the drain current of the transistor.[34] Other methods to limit the drain current include the use of a unipolar barrier, MIS barrier, and space charge limited barrier.[2] Among these methods, the Schottky barrier method is the simplest. By changing the height of the barrier by varying the gate electric field, the magnitude of the drain current is changed. In Figure 3, we have drawn a distinction in

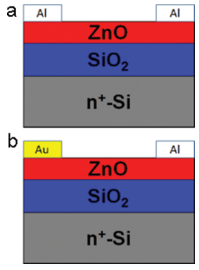

Figure 3. Structure of (a) typical symmetrical ZnO TFT on a Si substrate and (b) asymmetrical TFT used in this work. In the symmetrical TFT, both contacts are ohmic. In the asymmetrical TFT, one contact is ohmic and another is a rectifying contact due to the Schottky barrier. When the Schottky junction is forward biased, the asymmetrical TFT behaves similar to the symmetrical TFT. When the Schottky junction is reverse biased, the behavior of the asymmetrical TFT diverges from that of the symmetrical TFT.

the back-gated configuration between the structure of a typical TFT with symmetrical source/drain electrodes and the asymmetrical SB-TFT, which is the subject of the present study. As shown in Figure 3, we used Al as the ohmic contact at the drain electrode and Au as the Schottky contact at the source electrode.

Figure 4 is a schematic diagram of the band line-up at the source-semiconductor-insulator interfaces. At zero gate bias (V_{GS}), the semiconductor is depleted of charge carriers near the source due to the presence of the Schottky barrier and its

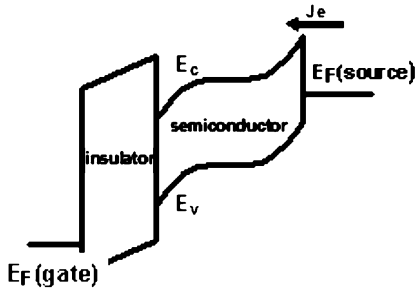

Figure 4. Source-semiconductor-insulator band diagram. When $V_{DS} > 0$ the Schottky contact will be reverse biased widening the depletion region, making the region around the source depleted from free charge carriers. Hence the amount of current will be independent of drain voltage (pinch off). By applying a positive voltage, the channel is formed by the accumulation of negative charge carriers.

accompanying depletion region. Therefore, the TFT is in the OFF-state at zero gate bias. The Schottky contact at the source is reverse-biased by the application of a positive drain bias (V_{DS}) and thus limits the injection of electrons from the source into the channel. Therefore, by applying a positive voltage at the drain, and increasing the same, the semiconductor near the source becomes further depleted of free charge carriers and the channel remains switched OFF. In this regime, the drain current becomes independent of the drain voltage and will only depend on the gate voltage. By applying a suitable positive voltage to the gate, the electrons are accumulated at the semiconductor-gate dielectric interface and the channel becomes conducting corresponding to the TFT being ON. The positive V_{DS} will increase the size of the depletion region under the source and cause it to extend to the semiconductor-gate dielectric interface as the drain voltage is increased. Hence no free charge carriers will be present in the semiconductor under the source. At this point the drain current saturates. As a result the drain voltage will have no further effect on the magnitude of the drain current. The Schottky barrier causes the transistor to saturate at lower voltages. Hence the transistor can operate at lower voltages which in turn reduces the power consumption.[35] It is well-known that the threshold voltage of polycrystalline ZnO TFTs shifts with time due to changes in the distribution of traps at grain boundaries and at the gate dielectric interface.[36] By making the threshold voltage dependent on the source injection barrier, such variations in the threshold voltage are circumvented. Furthermore, because a positive gate voltage is required to make the channel conductive, the device operates in enhancement mode.

3.3. Electrical Characteristics of ZnO SB-TFTs. Figure 5 shows the electrical characteristics of Schottky TFTs for different gate voltages and device dimensions. In Figure 5a, the I_D-V_{DS} characteristic of a device with channel length of 20 μm and width of 100 μm is plotted for both negative and positive values of the drain voltage. Unlike a regular TFT, which is expected to exhibit symmetrical characteristics for $\pm V_{DS}$, the *n*-ZnO SB-TFT fabricated by us exhibits highly unsymmetrical *I*−*V* characteristics. At negative V_{DS}, the Au-ZnO Schottky barrier at the source is forward biased and there is a very small barrier to injection. Furthermore, the ZnO films formed by us are heavily *n*-doped, as will be shown below. Consequently, except for a small region of sublinear slope at low V_{DS}, the I_D-V_{DS} characteristics are linear like those of a simple resistor when the Au-ZnO junction is forward biased. In contrast, for positive V_{DS}, the Au-ZnO junction is reverse-biased and the *I*−*V* characteristics are those of a transistor for lower drain source voltages. Likewise, the SB-TFT with a channel length of 50 μm and a width of 200 μm in Figure 5**b** shows a nearly ideal transistor characteristic at positive V_{DS}. The slope of I_D-V_{DS} is very small in the saturation region, which indicates that the transistor is in hard saturation. This proves that the transistor has high output impedance which is a desirable feature for most applications. Additional plots of the I_D-V_{DS} characteristics of devices with channel lengths of 35 and 10 μm respectively are provided in Figures S1 and S2 in the Supporting Information. From Figures 5a, b and Figures S1 and S2 in the Supporting Information, it is clear that each device has two points in reverse bias at which its behavior changes. One point is the drain voltage (V_{DSat}) at which the drain current saturates. Another point is the voltage at which the saturated drain current begins to sharply increase again (V_{Rt}). The lateral electric field in the channel for the same drain voltage increases

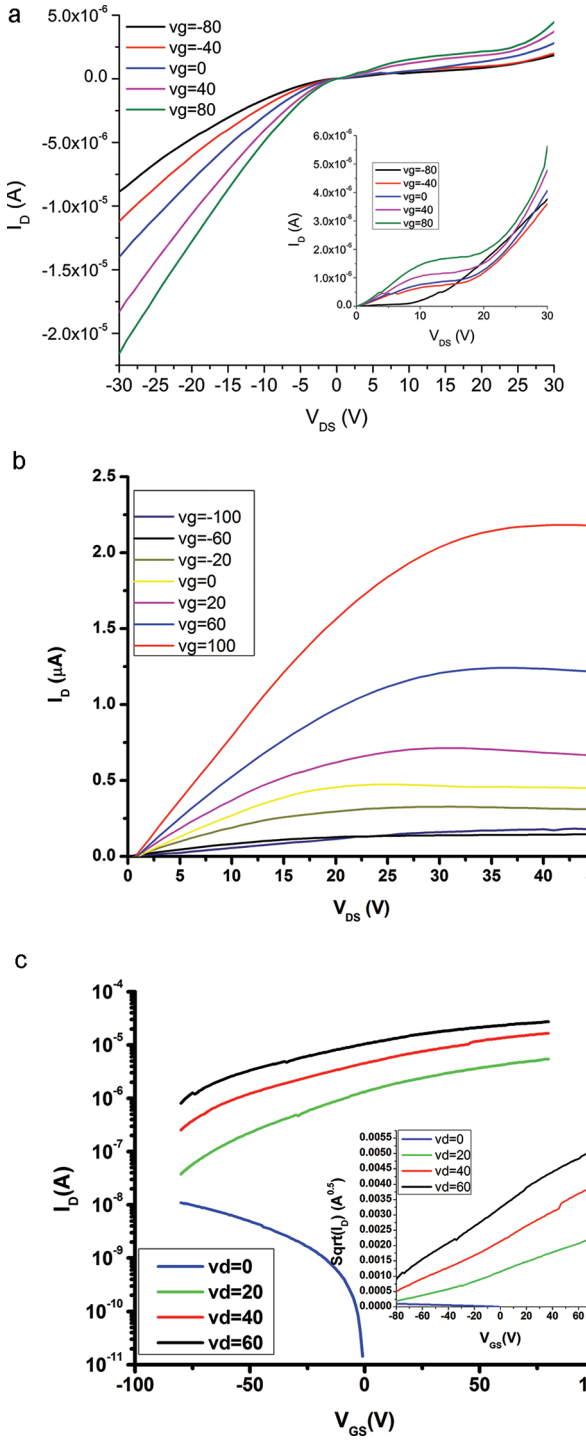

Figure 5. I_D-V_{DS} characteristics of solution-processed asymmetric ZnO TFTs with an Au Schottky contact and an Al ohmic contact (a) I_D-V_{DS} of TFT with channel length (L) = 20 μm, W = 100 μm with inset showing the characteristics of a similar device with identical dimensions under positive drain bias and (b) I_D-V_{DS} of TFT with channel length (L) = 50 μm, W = 200 μm, (c) Log scale for I_D-V_{GS} of TFT with channel length (L) = 50 μm, W = 200 μm. The inset shows the $(I_D)^{1/2}-V_{GS}$ curve. A mobility of 0.01cm^2/(V s) was calculated from the $(I_D)^{1/2}-_{GS}$ curve.

with decreasing channel length. This causes lower channel length devices to saturate at smaller values of the drain voltage (lower V_{DSat}) and allows the reverse tunneling currents to reassert themselves at smaller values of the drain voltage (lower V_{Rt}). Thus at channel lengths at the lower end of the range used in our study, contact effects dominate the transport and the influence of the gate is reduced. Figure 5c shows the I_D-V_{GS} characteristic, which shows an on/off current ratio of 100. The behavior of the TFT at V_{DS} = 0 is different from other values of drain-source voltage. This is because when V_{DS} = 0 the only voltage that affects the Schottky barrier is the V_{GS} voltage. As V_{GS} decreases, the barrier height reduces resulting in an increase in the current. However when a positive value of V_{DS} is applied, the drain bias dominates the behavior of the Schottky contact, making it reverse biased. As the V_{GS} increases in this case, more negative charge carriers are accumulated in the channel and the current increases. A threshold voltage of −110 V and a saturation mobility of 0.01 cm^2/(V s) were extracted from the slope of $(I_D)^{1/2}-V_{GS}$ characteristic (Figure 5c). A linear mobility of 5.7 × 10^{-3} was obtained from the transconductance curve (explained in Figure S3 in the Supporting Information).

As mentioned previously, the ZnO TFT behaves as a resistor when the Schottky barrier is forward biased. The channel conductance and resistivity extracted from the linear I_D-V_{DS} characteristic is shown in Figure 6a. Here, the channel conductance actually refers to the conduction of the channel while the resistivity refers to the ZnO film. The channel

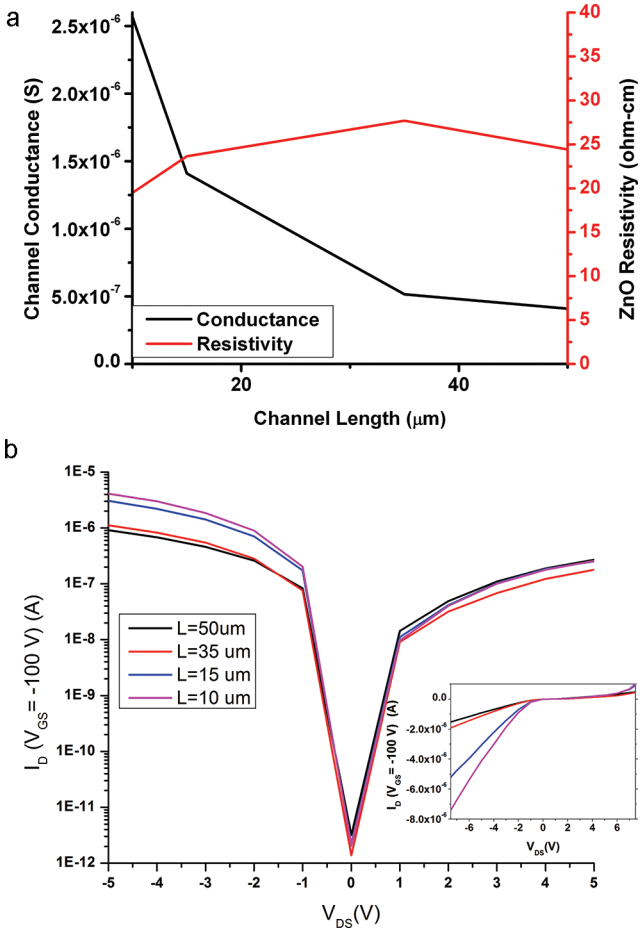

Figure 6. (a) Channel conductance and resistivity as a function of channel length at zero gate bias. (b) Drain current for different channel length devices as a function of drain voltage at a gate bias of −100 V (inset) shows the same data on a linear scale. All devices had a channel width of 100 μm.

dx.doi.org/10.1021/am201656h | ACS Appl. Mater. Interfaces 2012, 4, 1423−1428

conductance and the film resistivity are two distinct parameters and the channel conductivity is not merely the reverse of the film resistivity. The channel conductance exhibits the expected decrease with increasing channel length and a curve fit is provided in Figure S4 in the Supporting Information. The resistivity of the ZnO film is obtained to be ~25 Ω-cm, which was also confirmed by four-point probe measurements. The near-constancy of the resistivity across different channel lengths points to uniform doping of the film. Using $\sigma = nq\mu$, and inserting the value of mobility obtained previously, the carrier concentration is obtained to be 2.5×10^{19} cm^{-3}, which indicates that the ZnO is heavily doped. Figure 6b, which plots the drain currents for devices of different channel lengths at the same gate bias, shows that the Au-ZnO Schottky junction provides rectification ratios of ~10−15. In general, Au is known to form leaky Schottky junctions with *n*-ZnO with rectification ratios of $\sim 1 \times 10^3$,[37] further accentuated in our case by the high doping of the ZnO, which causes tunneling through the barrier to dominate thermionic emission.[38] Thus in Figure 5a, we observe that at high positive drain bias, the tunneling-induced reverse leakage current becomes large enough to overpower the transistor behavior and thereby dominate the *I*−*V* characteristic.

As can be seen from Figure 5, the Schottky barrier causes the transistor to saturate at lower gate voltages. Because of the low threshold voltage of −110 V, the transistor turns off at gate biases lower than −110 V which we can not apply to the gate due to instrument limitations. This shows that the transistor is an n-type depletion mode transistor since negative voltage is needed to turn the device off. Our best devices yielded on/off current ratios of $\sim 1 \times 10^3$. The reason behind both the low on/off current ratio and the low threshold voltage is the high doping level of ZnO (2.5×10^{19} cm^{-3}) High doping increases the charge carrier tunneling thus increasing the leakage current. Since charge injection from the source into the channel is controlled by tunneling, the width of the barrier plays an important role along with the height of the barrier. In our device configuration, the gate bias modulates not only the resistance of the ZnO in the channel region but also modulates the resistance of the rectifying contact. When the Schottky junction is reverse biased, the gate voltage modulates the conductance of the channel as follows:[39] at gate bias lower than the threshold voltage, the width of the tunneling barrier is significant and injection from the source is limited because of the confinement of electrons by the Schottky barrier − this corresponds to the OFF state; at gate bias larger than the threshold voltage, the width of the tunnel barrier is reduced by the gate electric field rendering the barrier nearly transparent thus allowing electron injection from the source by field emission − this corresponds to the ON state. Despite the high doping level of the ZnO and the poor rectification provided by the Au-ZnO junction, SB-TFTs allowed control over the electrical characteristics which approached ideal transistor behavior. The effectiveness of the asymmetrical SB-TFT concept is thus demonstrated. Our results clearly indicate that moderately doped ZnO coupled with strongly rectifying contacts could be used to change the threshold voltage of ZnO devices and achieve stable enhancement mode operation.

4. CONCLUSION

Heavily doped ZnO thin films with a carrier concentration of 2.5×10^{19} cm^{-3} were fabricated by solution processing. The films did not possess the commonly obtained [002] preferred orientation. The use of triethylamine as the stabilizer is relatively novel and had a dramatic impact on the structural and electrical properties of the ZnO films, thus pointing to importance of the stabilizer in sol−gel ZnO synthesis. The obtained ZnO films were used as active layers in asymmetrical thin film transistors wherein the ohmic contact at the source was replaced by a Schottky contact (Au). When the Schottky contact was reverse biased, the field-effect of the gate could modulate the conductance of the channel even though the ZnO constituting the channel material was heavily doped and the Au-ZnO Schottky contact had low rectification ratios. A proof-of-concept demonstration of the effectiveness of the source injection barrier in controlling the electrical characteristics of ZnO devices was provided. The SB-TFT concept is shown to have great promise for engineering enhancement mode devices and adjusting the threshold voltage without p-type doping.

■ ASSOCIATED CONTENT

Supporting Information

Additional figures and equations (PDF). This material is available free of charge via the Internet at http://pubs.acs.org.

■ AUTHOR INFORMATION

Corresponding Author

*E-mail: kshankar@ualberta.ca.

Notes

The authors declare no competing financial interest.

■ ACKNOWLEDGMENTS

This work was supported by the Natural Sciences and Engineering Research Council (NSERC) of Canada, the Alberta nanoBridge and the Canadian Institute for Photonic Innovations (CIPI). Some device fabrication and testing used research infrastructure made possible by a Leaders Opportunity Fund grant to K.S. from the Canada Foundation for Innovation (CFI) and the Alberta Small Equipment Grants Program (SEGP). We thank the staff at the University of Alberta NanoFab. The authors also acknowledge Shiraz Merali and the University of Alberta Integrated Nanosystems Research Facility (INRF) for assistance with X-ray diffraction. We thank Xiaojiang Zhang and the National Research Council−National Institute of Nanotechnology (NRC-NINT) for assistance with FESEM imaging.

■ REFERENCES

(1) Look, D. C. *Mater. Sci. Eng., B* **2001**, *80* (1−3), 383−387.
(2) Brillson, L. J.; Lu, Y. C. *J. Appl. Phys.* **2011**, *109* (12), 121301.
(3) Anderson, J.; Chris, G. V. d. W. *Rep. Prog. Phys.* **2009**, *72* (12), 126501.
(4) Cheng, H.-C.; Chen, C.-F.; Tsay, C.-Y. *Appl. Phys. Lett.* **2007**, *90* (1), 012113−3.
(5) Ryu, Y.; Lee, T.-S.; Lubguban, J. A.; White, H. W.; Kim, B.-J.; Park, Y.-S.; Youn, C.-J. *Appl. Phys. Lett.* **2006**, *88* (24), 241108−3.
(6) Wolff, K.; Hilleringmann, U. *Solid-State Electron.* **2011**, *62* (1), 110−114.
(7) Sun, B.; Sirringhaus, H. *Nano Lett.* **2005**, *5* (12), 2408−2413.
(8) Mourey, D. A.; Park, S. K.; Zhao, D. L. A.; Sun, J.; Li, Y. Y. V.; Subramanian, S.; Nelson, S. F.; Levy, D. H.; Anthony, J. E.; Jackson, T. N. *Org. Electron.* **2009**, *10* (8), 1632−1635.
(9) Ohyama, M.; Kouzuka, H.; Yoko, T. *Thin Solid Films* **1997**, *306* (1), 78−85.
(10) Ozgur, U.; Hofstetter, D.; Morkoc, H. *Proc. IEEE* **2010**, *98* (7), 1255−1268.

(11) Park, J. S.; Jeong, J. K.; Mo, Y. G.; Kim, H. D.; Kim, C. J. *Appl. Phys. Lett.* **2008**, *93* (3).
(12) Moon, Y. K.; Moon, D. Y.; Lee, S.; Park, J. W. *Nucl. Instrum. Methods Phys. Res., Sect. B* **2010**, *268* (16), 2522−2526.
(13) Park, J. S. *J. Electroceram.* **2010**, *25* (2−4), 145−149.
(14) Remashan, K.; Choi, Y. S.; Park, S. J.; Jang, J. H. *Jpn. J. Appl. Phys.* **2011**, *50* (4).
(15) Trinh, T. T.; Nguyen, V. D.; Ryu, K.; Jang, K.; Lee, W.; Baek, S.; Raja, J.; Yi, J. *Semicond. Sci. Technol.* **2011**, *26* (8).
(16) Moon, Y. K.; Moon, D. Y.; Lee, S.; Lee, S. H.; Park, J. W.; Jeong, C. O. *J. Vac. Sci. Technol. B* **2008**, *26* (4), 1472−1476.
(17) Tsay, C. Y.; Fan, K. S. *Mater. Trans.* **2008**, *49* (8), 1900−1904.
(18) Zhu, J.; Chen, H.; Saraf, G.; Duan, Z.; Lu, Y.; Hsu, S. T. *J. Electron. Mater.* **2008**, *37* (9), 1237−1240.
(19) Ponce, M. A.; Ramirez, M. A.; Parra, R.; Malagù, C; Castro, M. C.; Bueno, P. R.; Varela, J. A. *J. Appl. Phys.* **2010**, *108* (7), 074505.
(20) Li, C. S.; Li, Y. N.; Wu, Y. L.; Ong, B. S.; Loutfy, R. O. *J. Mater. Chem.* **2009**, *19* (11), 1626−1634.
(21) Kim, Y. S.; Tai, W. P.; Shu, S. J. *Thin Solid Films* **2005**, *491* (1−2), 153−160.
(22) Wang, M. R.; Wang, J.; Chen, W.; Cui, Y.; Wang, L. D. *Mater. Chem. Phys.* **2006**, *97* (2−3), 219−225.
(23) Ghosh, R.; Paul, G. K.; Basak, D. *Mater. Res. Bull.* **2005**, *40* (11), 1905−1914.
(24) Castanedo-Perez, R.; Jimenez-Sandoval, O.; Jimenez-Sandoval, S.; Marquez-Marin, J.; Mendoza-Galvan, A.; Torres-Delgado, G.; Maldonado-Alvarez, A. *J. Vac. Sci. Technol. A* **1999**, *17* (4), 1811−1816.
(25) Wang, M.; Kim, E. J.; Chung, J. S.; Shin, E. W.; Hahn, S. H.; Lee, K. E.; Park, C. *Phys. Status Solidi A* **2006**, *203* (10), 2418−2425.
(26) Srinivasan, G.; Gopalakrishnan, N.; Yu, Y. S.; Kesavamoorthy, R.; Kumar, J. *Superlattices Microstruct.* **2008**, *43* (2), 112−119.
(27) Bahadur, H.; Srivastava, A. K.; Sharma, R. K.; Chandra, S. *Nanoscale Res. Lett.* **2007**, *2* (10), 469−475.
(28) Dutta, M.; Mridha, S.; Basak, D. *Appl. Surf. Sci.* **2008**, *254* (9), 2743−2747.
(29) Jones, A. C.; Wright, P. J.; Cockayne, B. *J. Cryst. Growth* **1991**, *107* (1−4), 297−308.
(30) Ong, B. S.; Li, C. S.; Li, Y. N.; Wu, Y. L.; Loutfy, R. *J. Am. Chem. Soc.* **2007**, *129* (10), 2750.
(31) Kamalasanan, M. N.; Chandra, S. *Thin Solid Films* **1996**, *288* (1−2), 112−115.
(32) Yoon, S. H.; Liu, D.; Shen, D. N.; Park, M.; Kim, D. J. *J. Mater. Sci.* **2008**, *43* (18), 6177−6181.
(33) Frenzel, H.; Lajn, A.; Brandt, M.; von Wenckstern, H.; Biehne, G.; Hochmuth, H.; Lorenz, M.; Grundmann, M. *Appl. Phys. Lett.* **2008**, *92* (19).
(34) Park, J.; Ozbek, A. M.; Ma, L.; Veety, M. T.; Morgensen, M. P.; Barlage, D. W.; Wheeler, V. D.; Johnson, M. A. L. *Solid-State Electron.* **2010**, *54* (12), 1680−1685.
(35) Shannon, J. M.; Gerstner, E. G. *IEEE Electron Device Lett.* **2003**, *24* (6), 405−407.
(36) Redinger, D. H. *IEEE Trans. Electron Devices* **2010**, *57* (12), 3460−3465.
(37) Frenzel, H.; Lajn, A.; von Wenckstern, H.; Biehne, G.; Hochmuth, H.; Grundmann, M. *Thin Solid Films* **2009**, *518* (4), 1119−1123.
(38) Lin, Y. J.; Jheng, M. J.; Zeng, J. J. *Appl. Surf. Sci.* **2010**, *256* (14), 4493−4496.
(39) Wang, C.; Snyder, J. P.; Tucker, J. R. *Appl. Phys. Lett.* **1999**, *74* (8), 1174−1176.